International Journal on Artificial Intelligence Tools
Vol. 21, No. 4 (2012) 1240016 (18 pages)

DOI: 10.1142/S0218213012400167

World Scientific
www.worldscientific.com

EVALUATION OF THE RISK OF STROKE WITH CONFIDENCE PREDICTIONS BASED ON ULTRASOUND CAROTID IMAGE ANALYSIS

ANTONIS LAMBROU
Computer Learning Research Centre, Royal Holloway, University of London, UK
a.lambrou@cs.rhul.ac.uk

HARRIS PAPADOPOULOS
Computer Science and Engineering Department, Frederick University, Cyprus
h.papadopoulos@frederick.ac.cy

EFTHYVOULOS KYRIACOU
Computer Science and Engineering Department, Frederick University, Cyprus
e.kyriacou@frederick.ac.cy

CONSTANTINOS S. PATTICHIS
Computer Science and Engineering Department, University of Cyprus, Nicosia, Cyprus
pattichi@ucy.ac.cy

MARIOS S. PATTICHIS
Electrical and Computer Engineering Department,
University of New Mexico, New Mexico, USA
pattichis@ece.unm.edu

ALEXANDER GAMMERMAN
Computer Learning Research Centre, Royal Holloway, University of London, UK
a.gammerman@cs.rhul.ac.uk

ANDREW NICOLAIDES
Imperial College London, UK, Vascular screening and Diagnostic Centre, London, UK
Cyprus Cardiovascular Disease Educational Research Trust, Nicosia, Cyprus
anicolaides1@gmail.com

Conformal Predictors (CPs) are Machine Learning algorithms that can provide reliable confidence measures to their predictions. In this work, we make use of the Conformal Prediction framework for the assessment of stroke risk based on ultrasound images of atherosclerotic carotid plaques. For this application, images were recorded from 137 asymptomatic and 137 symptomatic plaques (symptoms are Stroke, Transient Ischaemic Attack (TIA), and Amaurosis Fugax (AF)). Two feature sets were extracted from the

plaques; the first based on morphological image analysis and the second based on image texture analysis. Both sets were used in order to evaluate the performance of CPs on this problem. Four CPs were constructed using four popular classification methods, namely Artificial Neural Networks (ANNs), Support Vector Machines (SVMs), Naive Bayes Classification (NBC), and k-Nearest Neighbours. The results given by all CPs demonstrate the reliability and importance of the obtained confidence measures on the problem of stroke risk assessment.

Keywords: Conformal prediction; confidence measures; assessment of stroke risk; atherosclerotic carotid plaques; ultrasound image analysis.

1. Introduction

Visual classification of high-resolution ultrasound has made the non-invasive visualisation of the carotid bifurcation possible, and has thus been used in the study of arterial wall changes. Clinical applications of carotid bifurcation ultrasound include: (i) identification and grading of stenosis of extracranial carotid artery disease often responsible for ischaemic strokes, Transient Ischaemic Attacks (TIAs) or Amaurosis Fugax (AF); (ii) follow-up after carotid endarterectomy; (iii) evaluation of pulsatile neck mass; (iv) investigation of asymptomatic neck bruits where severe internal carotid artery stenosis is used as a predictive factor for future stroke; (v) cardiovascular risk assessment where the presence of carotid bifurcation of atherosclerotic plaques is associated with increased cardiovascular mortality. During the last 20 years, the introduction of computer aided methods and image standardisation has improved the objective assessment of carotid plaque echogenicity and heterogeneity,[1] and has largely replaced subjective assessment that had been criticised for its poor reproducibility.[20]

Until now several studies presenting classification models for carotid ultrasound images have been presented, see for example Refs. 5, 10, 12, 19, but none of these methods provide any valid confidence measures on this problem. In order to address this, we have proposed the use of Conformal Prediction[32] in a previous study,[16] where Conformal Prediction was used to assess the risk of stroke based on morphological ultrasound images. Conformal Predictors (CPs) can provide prediction regions which guarantee, under the i.i.d. assumption, that the error rate of these regions will be bounded by a desirable significance level. For example, if the confidence level is 95%, then the error rate will not exceed the 5% that is expected in the long run.

In this work, we extend our work presented in Ref. 16 by examining datasets with both morphological and texture features. Our system is based on a set of morphological features and a set of classical image texture features, extracted from 274 ultrasound images of carotid plaques. Images used are base-line images, which means that they were collected before any event happened. From these images, 137 were classified as asymptomatic, while 137 are symptomatic (an event of Stroke, Transient Ischaemic Attack (TIA) or Amaurosis Fugax (AF) happened). We apply the Conformal Prediction framework on both categories of features, using four dif-

ferent classifiers: Artificial Neural Network (ANN); Support Vector Machine (SVM); Naive Bayes Classifier (NBC); and k-Nearest Neighbours (k-NN). We compare the results and show the reliability and practicality of the confidence measures obtained for the classification of atherosclerotic carotid plaques.

The rest of the paper is structured as follows. In section 2, we give a brief review of the relevant literature. In section 3, we describe the data used, we give an overview of the Conformal Prediction framework, and explain how we have transformed four machine learning classifiers into CPs. In section 4, we describe our experimental settings and we give results. Moreover, we discuss and compare our results with the results in Refs. 14 and 5 which have conducted previous studies on the same data. In section 5, we conclude and outline our future work.

2. Related Work

Several efforts for automatic classification of ultrasound carotid plaque images have been developed over the years (see Ref. 12). Earlier studies have been primarily focused on basic statistical features such as the gray scale median (GSM), the mean, the median, the standard deviation, skewness and Kurtosis. In these earlier studies, the GSM was found to be very successful in differentiating between symptomatic and asymptomatic cases. Depending on the image pre-processing method, threshold values for the GSM were provided for differentiating between symptomatic and asymptomatic cases. Here, brighter plaques tended to be asymptomatic.[12] Standard texture features have been extensively used for the classification of carotid plaques. More recently, we have the introduction of morphological features that have given promising results. The most successful morphological features were based on a multi-level decomposition that are associated with different plaque image components. In the multi-level approach, each normalized plaque is thresholded at three different intensity ranges (low, medium, high). The darkest (low) components are associated with unstable plaque components such as lipid and hemorrhages. On the other hand, more stable plaque components are captured at higher brightness levels.[12]

Conformal Prediction (CP)[32] is a novel technique for obtaining reliable confidence measures. The technique was first proposed in Ref. 8 and later improved in Refs. 30 and 31. CPs are built using classical machine learning algorithms, called underlying algorithms. CPs complement the predictions of the underlying algorithms with measures of confidence. Many CPs have been built to date, based on various algorithms such as Support Vector Machines,[30] k-Nearest Neighbours for classification[29] and for regression,[26] Random Forests,[6] and Genetic Algorithms.[15] The computational efficiency of CPs has also been greatly improved using Inductive Conformal Prediction (ICP),[22] as demonstrated in applications to Ridge Regression,[25] k-Nearest Neighbours,[27] and more recently in applications to Neural Networks.[28,24] The CP framework has been successfully applied to medical problems, such as ovarian cancer diagnosis,[3] breast cancer diagnosis,[9] classification of leukaemia subtypes,[2] and acute abdominal pain diagnosis.[23]

Other approaches that can provide some kind of confidence measures include Bayesian methods and the Probably Approximately Correct (PAC) theory. Nevertheless, these approaches have some important drawbacks that can hinder application. For Bayesian theory, *a priori* assumptions need to be made about the data. If prior knowledge is not available, and especially for limited data sets, the Bayesian estimated confidence intervals can be misleading. For example, at the 95% of confidence, the error rate can be much more than the expected 5%. An elaborate comparison of the Bayesian framework with Conformal Prediction is made in Ref. 18. In the case of applying PAC theory, the data used must be particularly clean, something that is not always true in practical applications. The weakness of the bounds of PAC methods is demonstrated in Ref. 21.

Several classification techniques have been used for the classification of carotid plaques, such as Multilayer Perceptron (MLP) Neural Networks,[19] Self Organizing Map (SOM) Networks,[5,4] Radial Basis Function (RBF) Networks, Probabilistic Neural Networks (PNNs), Support Vector Machines (SVMs)[13,14] and k-Nearest Neighbours.[5,4] In addition, research has been done on simple statistical analysis of the plaque characteristics.[10,7,11,33] For validation, the leave-one-out method is commonly used. Receiver operating characteristic (ROC) curves have also been used for measuring performance.[5,19] A summary of these methods can be found in Ref. 12.

3. Material and Methods

3.1. *Atherosclerotic carotid plaque data*

A total of 274 carotid plaque ultrasound images associated with retinal or hemispheric symptoms (33 stroke, 60 TIA, and 44 AF) were used in this work. Patients with cardioembolic symptoms or distant symptoms (more than 6 months) were excluded from the study. Asymptomatic plaques were truly asymptomatic if they had never been associated with symptoms in the past, or symptomatic if they had been associated with retinal or hemispheric symptoms (Stroke, TIA or AF). The ultrasound images were collected in the Irvine Laboratory for Cardiovascular Investigation and Research, Saint Mary's Hospital, UK, using an Advanced Technology Laboratories (ATL model HDI 3000, Seattle, USA) duplex scanner with a linear broadband width 4–7 MHz (multifrequency) transducer, at a resolution of 20 pixels/mm. The gray scale images (gray levels 0–255) were normalized manually by adjusting the image linearly. The plaque identification and segmentation tasks are quite difficult and were carried out manually by a physician or vascular ultrasonographer who are experienced in scanning, both actions are described in Ref. 17.

3.1.1. *Texture features*

Texture features, shape parameters, and morphological features were extracted from the manually segmented ultrasound plaque images. Seven different texture features sets were extracted from the plaque segments using the algorithms described in

Ref. 5. The algorithms used in these studies namely are (1) Statistical Features (SF), (2) Spatial Gray Level Dependence Matrices (SGLDM), (3) Gray Level Difference Statistics (GLDS), (4) Neighbourhood Gray Tone Difference Matrix (NGTDM), (5) Statistical Feature Matrix (SFM) method, (6) Laws Texture Energy Measures (TEM), (7) Fractal Dimension Texture Analysis (FDTA), (8) Fourier Power Spectrum (FPS) features, (9) Run Length Statistics (RUNL).

3.1.2. *Morphological features*

Morphological features are motivated from the need to study the basic structure of the plaque. We have used two morphological analysis methods in order to quantify morphological features of the plaques. The first one was based on a multilevel approach where the image intensity was thresholded at three different levels, while the second one was based on gray scale morphological analysis.

Morphological features of plaques are strongly associated with events. For example black (echolucent) plaques with white big blobs are considered to be very dangerous. From a structural perspective, morphological methods allow us to provide size distributions for different components of the plaque. A detailed analysis of morphological features extracted from the plaques can be found in Ref. 14. In this work, we have used the group of L-images as described in Ref. 14. This group gave the best accuracy results.

3.2. *Conformal prediction*

Provided a training dataset, Conformal Predictors (CPs) output predictions for new instances together with valid confidence measures, based on the assumption that the data are identically and independently distributed (i.i.d.). Additionally, CPs can provide prediction regions (more than one possible predictions for a new instance), such that the error rate of the prediction regions will not exceed a given significance level in the long run. We explain how this is done in the following paragraphs.

A training set is of the form $\{(x_1, y_1), \ldots, (x_n, y_n)\}$, where x_i is a vector of real-valued attributes and $y_i \in \{Y_1, Y_2, \ldots, Y_c\}$ is a label given to the instance x_i. Given a new instance x_{n+1}, we intend to predict the label y_{n+1} (i.e. the class of the instance). In order to make a prediction, we assume all possible labels $Y_h \in \{Y_1, Y_2, \ldots, Y_c\}$ of the new instance, and we test for each assumed label the likelihood of being correct. To get the likelihood of each assumption, we append the new instance x_{n+1} in our training set together with the assumed label Y_h, and we train an underlying classical machine learning algorithm on the extended training set

$$\{(x_1, y_1), \ldots, (x_{n+1}, Y_h)\}\,. \tag{1}$$

The learning algorithm builds a model about the data and is able to make predictions. A CP employ a non-conformity measure based on the derived model to calculate a non-conformity score for each of the instances in (1). A non-conformity score indicates how different (or strange) an instance x_i is for its given label y_i,

compared to the other instances in (1). In section 3.3, we explain how we have used four classical machine learning algorithms in order to generate non-conformity scores. The CP compares the non-conformity score of the new instance with the rest of the non-conformity scores in the training set. If the assumed label is correct, we expect to get a low non-conformity score for the new instance (a score that is comparable with the rest). We use the following p-value function to calculate how likely the assumed label is of being correct:

$$p(Y_h) = \frac{\#\{i = 1, \ldots, n+1 : a_i \geq a_{n+1}\}}{n+1}, \tag{2}$$

which compares the non-conformity score a_{n+1} of (x_{n+1}, Y_h) with all the other non-conformity scores of the rest of the instances in the extended training set. We call the output of this function the p-value of the class Y_h.

Given the true label y_{n+1}, the p-value function in (2), satisfies the following property for all probability distributions P, and for any significance level ϵ:

$$P(p(y_{n+1}) \leq \epsilon) \leq \epsilon\,. \tag{3}$$

In fact, the p-value function is a test function which measures how likely the dataset is of being i.i.d. If the p-value is lower than a given ϵ, it is because we either have non i.i.d. data, or because some event has happened with probability less than or equal to ϵ. Based on the assumption that our data are i.i.d., we know that if we include in our predictions all assumed labels that provide a p-value greater than a given significance level ϵ, then the probability of missing the true label of an instance will be less than or equal ϵ. In the case that all p-values are less than ϵ we then include the label with the highest p-value to ensure that our regions will always contain at least one prediction. This step does not increase the probability of error. The definition of a prediction region is given as

$$R = \{Y_h : p(Y_h) > \epsilon\} \cup \left\{ arg \max_{h=1,\ldots,c} (p(Y_h)) \right\}. \tag{4}$$

Our predictions are now called prediction regions, since they may contain more than one possible labels. In the long run, these regions will make errors at a rate of at most ϵ. Therefore, we have $1-\epsilon$ confidence in these predictions. Optionally, we may output only a single label (forced prediction) instead of a prediction region. That is, we output the label with the highest p-value as the prediction together with a confidence measure which is 1 minus the second largest p-value. The confidence measure indicates how likely the prediction is of being correct, with respect to the rest of the labels.

In Table 1, we give an example of a prediction region which contains a single label and a prediction region which contains both labels for the 95% level of confidence ($\epsilon = 0.05$). We call a prediction region which contains only one label a certain prediction. That is, the algorithm can be certain for its prediction at the required

Table 1. Example of prediction regions for 95% level of confidence ($\epsilon = 0.05$) and forced predictions with confidence measures.

Instance	$\mathbf{x_1}$	$\mathbf{x_2}$
$\mathbf{p(Y_1)}$	0.8623	0.1920
$\mathbf{p(Y_2)}$	0.0145	0.3768
Actual label	Y_1	Y_2
Prediction region for $\epsilon = 0.05$	$\{Y_1\}$	$\{Y_2, Y_1\}$
Forced prediction	$\{Y_1\}$	$\{Y_2\}$
Confidence	98.55%	80.80%

level of confidence. For the instance x_1, the second p-value is 0.0145, which is less than the significance level 0.05. Therefore, we can discard the second label at 95% level of confidence and give a certain prediction, which is the label that gives the highest p-value. In contrast, for instance x_2, the second largest p-value is 0.1920 and is greater than the significance level. In this case, the second largest p-value cannot be discarded and thus we give an uncertain prediction region with both possible labels for the given level of confidence. If we decrease the confidence level to 80.80% (or lower), we then have a certain prediction (or forced prediction), but the low confidence in this case is an indication that the prediction may require more consideration.

3.3. *Non-conformity measures*

A non-conformity measure is a way of scoring how strange a new instance is for its label compared with other instances that are given in a training set. Every non-conformity measure that we derive determines a Conformal Predictor (CP), and is used in (2) in order to calculate p-values. In this section, we describe how we derive non-conformity measures using Artificial Neural Networks (ANNs), Support Vector Machines (SVMs), Naive Bayes Classification (NBC), and k-Nearest Neighbours.

3.3.1. *Artificial neural networks*

Artificial Neural Networks (ANNs) are networks of interconnected neurons. Each connection is associated with a weight which determines the intensity of the signal traveling through that connection. These weights are adjusted during training to reduce the output error of the network. The output layer of a neural network has a neuron o_j for each possible class, and given an instance x_i we predict the class Y_j corresponding to the output neuron which gives the highest value.

We expect that the more conforming an instance is for its given label, the higher the corresponding o_j value would be. As proposed in Ref. 28, we can build a CP based on ANNs (ANN-CP) using the non-conformity measure

$$a_i = 1 - o_t \,, \tag{5}$$

for any (x_i, y_i) where $y_i = Y_t$, and $o_t = [0, 1]$. Alternatively, we can use the following non-conformity measure which is again defined in Ref. 28:

$$a_i = \frac{max_{j=1,\ldots,c:j\neq t} o_j}{o_t} \,. \tag{6}$$

That is, we use as a numerator the maximum of the output units which do not correspond to the label of the given instance, since a higher value from such units also indicates a more strange instance and would give a higher non-conformity score when divided by o_t.

3.3.2. *Support vector machines*

Support Vector Machines (SVMs) identify boundary instances for each class, and fix a separating hyperplane that maximises the margin between them. In the case of a non-linear separation, SVMs use a kernel mapping function, where the instances are mapped to a higher dimensional space such that a linear separation can be made. For the purpose of building a CP using SVM (SVM-CP), we use the distance of each instance from the separating hyperplane together with the class that it belongs to, in order to produce non-conformity scores. For $Y = \{-1, 1\}$, we use the non-conformity measure

$$a_i = -y_i h(x_i) \,, \tag{7}$$

where $h(x_i)$ is the output of the SVM for the given instance x_i. The output $h(x_i)$ is negative if the instance belongs to class -1, and positive if it belongs to class 1. If the prediction is correct, then the further the instance is from the hyperplane, the less the non-conformity score will be. In contrast, if the prediction is incorrect, the non-conformity score will increase as the distance from the hyperplane increases.

The original SVM works only for binary classification problems. In this work, we have optionally used a more general SVM-CP (defined in Ref. 32), which can work for both binary and multi-class problems. We have used the one-against-the-rest procedure, which transforms a multi-class problem into several binary sub-problems. A class is selected for each sub-problem, and the instances are labeled with $\{-1, 1\}$ depending on whether they belong to the selected class. A non-conformity score is generated for each instance in each sub-problem, using (7). Finally, the average of the scores of each instance is calculated to get a final non-conformity measure.

3.3.3. *Naive Bayes Classifier*

The Naive Bayes Classifier (NBC) is named after Bayes' Theorem, and the "naive" assumption of attribute independence. The assumption that attributes are independent is a simplistic one. Nevertheless, Naive Bayes works very well on many real-world datasets, particularly when combined with attribute selection procedures that remove redundant, and hence nonindependent, attributes. The classifier multiplies the probabilities of the attributes given their class, and outputs the probability

of label y_i given instance x_i. We can use the output probability to define a non-conformity measure and build a CP based on the NBC (NBC-CP):

$$a_i = 1 - P(y_i|x_i)\,. \tag{8}$$

As $P(y_i|x_i)$ increases the example is less strange, since the probability assigned by the NBC to the correct class is higher.

3.3.4. *Nearest Neighbours*

The k-Nearest Neighbours (k-NN) method computes the distance of a test instance from the other instances that are provided in the training set, and finds its k nearest instances. The prediction of the algorithm is the class of the majority of the k instances. In the case of building a CP based on k-NN (k-NN-CP), we use the distances of the k nearest instances to define a non-conformity measure. The simplest approach is to calculate the total of distances of the k instances that belong to the class of instance x_i, since the nearer the instance is to its class, the less strange it is. Nonetheless, for a more accurate non-conformity measure we also take into consideration the distances of the k nearest instances that belong to other classes, since the nearer the instance x_i is to the other classes the more strange it is. We build our k-NN-CP using the non-conformity measure defined in Refs. 29 and 27:

$$a_i = \frac{\sum_{j=1,\ldots,k} s_{ij}}{\sum_{j=1,\ldots,k} o_{ij}}\,, \tag{9}$$

where s_{ij} is the jth shortest distance of x_i from the instances of the same class, and o_{ij} is the jth shortest distance of x_i from the instances of other classes.

4. Experiments

We have experimented on both the morphological data and the texture data described in section 3.1, and we have compared the results of all the CPs as defined in section 3.3. Before conducting our experiments we have applied Principal Component Analysis (PCA) on the datasets and selected the features which accounted for 98% of each dataset's variance. For evaluating our algorithms, we have applied the Leave-One-Out Cross Validation (LOOCV) technique. Both of these choices were made in order to be able to have similar results with Ref. 14 which have conducted research on the morphological data. In LOOCV, a test instance is left out from the training set and after training a prediction is made for the left-out instance. This experiment is repeated for every instance in the dataset, and the predictions are then evaluated with the true labels of the instances. The ANN-CP was structured with one hidden layer, and all units had sigmoid activation functions. We have used a learning rate of 0.3 and a momentum rate of 0.2. In each experiment, the ANNs were trained for 500 epochs with 10% validation set, which was used to stop training when the performance on the validation set was deteriorating. For the SVM-CP, we have used a Radial Basis Function (RBF) kernel mapping.

4.1. *Results*

In Table 2, we show the results of the four CPs described in section 3.3 on the morphological data. We have conducted experiments with different parameter values of the underlying algorithm of each CP. The parameter for the ANN-CP is the number of neurons of the hidden layer, for the SVM-CP the spread of the RBF kernel, and for the k-NN-CP we set the number of nearest neighbours considered. We should note here that the NBC-CP (also included in Table 2) has no parameters. We also report the certainty and error rates of each CP for the confidence levels 95%, 85%, and 75%. The certainty rates correspond to the prediction regions that contained only a single label, and the error rates correspond to the prediction regions that did not contain the true label. The certainty rates show the efficiency of each CP. High rates of certainty show a better quality in our confidence measures. We highlight the results which give the best average percentage of accuracy and certainty rates.

In Table 3, we compare the accuracy results of the four CPs with the results of the corresponding classical algorithms. We have selected for each algorithm the parameters which are highlighted in Table 2. We have also calculated the True Positive Rates (TPR), and True Negative Rates (TNR). A TN in our case is a plaque which has been correctly classified as asymptomatic, and a TP a plaque which is correctly classified as symptomatic.

In Table 4, we give the results of the CPs on the texture data. The structure of the results is identical to that of Table 2. In Table 5, we compare the accuracy, TPR and TNR of the classical algorithms with the corresponding CPs.

4.2. *Discussion*

As expected, the error rates confirm the validity of the CPs as they are always near the pre-set significance levels, regardless of the non-conformity measures defined and parameters that have been chosen for each algorithm. On the morphological data, the ANN-CP provides the best average of accuracy and certainty rates compared with the rest of the CPs, and the results are improved even more when the size of the hidden layer is limited to a single neuron. At 95% level of confidence the ANN-CP gives 35.04% of certain prediction regions. This means that a significant amount of patients will get a prediction in which the error will not exceed the 5% that is allowed. Given the difficulty of the task, this is arguably a useful result. Moreover, as we decrease the confidence level, the certainty rates increase dramatically.

The accuracy between the classifiers and their corresponding CPs have no significant difference, as expected. We highlight here that our aim is not to improve accuracy. We show that CPs can provide more information in each prediction while accuracy is retained. As shown in Table 3, all algorithms provide higher TPRs and lower TNRs on the morphological data. This means that patients with symptomatic plaques will have more chance to be identified, whereas asymptomatic plaques could be miss-classified as symptomatic. This kind of wrong predictions could yield unnecessary complications, such as surgery, in which other risks may be introduced. For

Table 2. Results of four CPs on the morphological data. For each parameter we show the accuracy, and the certainty and error rates for three levels of confidence (95%, 85%, and 75%). We highlight the best results which are given by the average percentage of the accuracy and the certainty rates.

		Certainty			**Error**		
CP	**Acc.**	**95%**	**85%**	**75%**	**95%**	**85%**	**75%**
ANN neurons							
0	73.36%	30.29%	67.15%	90.15%	4.74%	13.50%	22.26%
1	**72.26%**	**35.04%**	**68.61%**	**89.42%**	**4.74%**	**14.23%**	**23.72%**
2	70.80%	32.48%	64.96%	88.32%	4.74%	14.23%	22.26%
3	71.90%	31.02%	68.98%	90.15%	4.74%	14.60%	23.36%
4	71.90%	32.85%	66.42%	88.69%	4.74%	13.87%	22.63%
5	71.53%	33.21%	66.42%	89.05%	5.11%	14.23%	22.63%
6	71.53%	34.31%	65.69%	88.32%	5.11%	13.50%	22.26%
7	71.90%	33.21%	65.69%	88.69%	4.74%	13.87%	22.63%
8	70.80%	31.75%	63.87%	87.96%	4.74%	14.60%	22.26%
9	70.80%	32.48%	64.96%	88.32%	4.74%	13.87%	22.63%
10	70.80%	33.94%	64.60%	88.69%	5.47%	13.50%	22.26%
SVM spread							
0.10	**73.72%**	**19.34%**	**54.74%**	**85.40%**	**4.74%**	**14.96%**	**24.82%**
0.11	73.72%	17.52%	54.38%	85.04%	4.74%	14.96%	24.82%
0.12	72.99%	18.61%	54.01%	85.40%	4.74%	14.96%	24.82%
0.13	72.99%	19.34%	54.38%	85.04%	4.74%	14.96%	24.82%
0.14	72.26%	20.44%	54.38%	85.77%	4.38%	14.96%	24.82%
0.15	72.26%	21.53%	54.74%	84.67%	4.74%	14.96%	24.82%
0.16	71.17%	21.17%	54.01%	85.04%	4.74%	14.96%	24.82%
0.17	70.80%	20.44%	54.74%	83.94%	4.74%	14.96%	24.82%
0.18	70.07%	21.17%	55.47%	83.94%	4.74%	14.96%	24.82%
0.19	69.71%	22.26%	55.84%	82.85%	4.74%	14.96%	24.82%
0.20	69.71%	22.99%	55.84%	82.12%	4.74%	14.96%	25.18%
k**-NN** k							
5	67.88%	28.83%	57.30%	82.48%	4.74%	14.96%	24.82%
6	67.52%	28.83%	56.57%	86.13%	4.74%	14.96%	24.82%
7	68.25%	29.20%	58.03%	87.59%	4.74%	14.96%	24.82%
8	69.71%	29.93%	56.93%	87.96%	4.74%	14.96%	24.82%
9	71.53%	29.20%	56.93%	87.23%	4.74%	14.96%	24.82%
10	71.53%	29.20%	56.57%	87.96%	4.74%	14.96%	24.82%
11	71.17%	29.20%	58.76%	87.96%	4.74%	14.96%	24.82%
12	70.44%	29.56%	59.12%	88.32%	4.74%	14.96%	24.82%
13	70.07%	29.56%	62.41%	88.32%	4.74%	14.96%	24.82%
14	**70.80%**	**29.56%**	**63.50%**	**89.05%**	**4.74%**	**14.96%**	**24.82%**
15	70.07%	29.20%	63.14%	89.78%	4.74%	14.96%	24.82%
NBC							
—	67.52%	21.90%	59.85%	81.75%	4.74%	14.96%	24.82%

Table 3. Comparing Accuracy, True Negative Rate (TNR), and True Positive Rate (TPR) of four classifier algorithms with the corresponding CPs, on the morphological data.

Method	Classifier			CP		
	Accuracy	**TNR**	**TPR**	**Accuracy**	**TNR**	**TPR**
ANN	71.16%	59.90%	82.50%	72.26%	60.06%	83.2%
SVM	73.72%	63.50%	83.94%	73.72%	63.50%	83.94%
NBC	68.24%	54.70%	81.80%	67.52%	63.64%	74.49%
***k*-NN**	70.07%	59.10%	81.00%	70.80%	58.39%	83.21%

this reason, a valid confidence measure in each prediction could play an important role for this application.

The accuracy on the texture data is slightly lower than that of the morphological data, but with no significant change in the certainty and error rates. As shown in Table 4, the best average of accuracy and certainty rates is again provided by the ANN-CP, which gives 71.53% accuracy and 34.31% certainty at the 95% level of confidence. The size of the hidden layer to achieve this result is set to 10 neurons, which is contrary to the size of a single neuron that has been set for the morphological data. This result suggests that the texture data is more complex than the morphological data. In order to achieve good results, the range of the parameters for the SVM-CP and k-NN-CP has been changed to a RBF parameter of $1 - 10$, and $k = 20, \ldots, 30$ respectively.

On the texture data, the TNR has increased in most of the algorithms, while the TPR has decreased (see Table 5). Therefore, more asymptomatic plaques are identified with the texture data, rather than symptomatic plaques. The miss-classification of a symptomatic plaque is critical for the patient, and thus again, a confidence measure in this kind of predictions seems to be important. It is remarkable that the NBC gives high TNR and low TPR, which is contradictory to what the rest of the algorithms give. The k-NN method gives a balanced result, where both TNR and TPR lie at about the same level. The results of the CPs are satisfactory, as the accuracy is preserved while extra information is provided.

In Table 6, we compare our accuracy on the morphological data with the results of Ref. 14, which describes work on the same data using identical experimental settings as ours. We also compare our accuracy results on the texture data with the results of Ref. 5. We would like to note that the dataset used in Ref. 5 is an older version of our dataset, which contains only 230 instances. Moreover, the experimental settings in Ref. 5 are slightly different than ours. Nevertheless, we are still able to show that the accuracy obtained here is very close to the best accuracy obtained in Ref. 5. We show the best accuracies achieved by the SVM and the Probabilistic Neural Network (PNN) classifiers used in Ref. 14, on the L-image group of the morphological data. We also include the results of our SVM and ANN CPs which are highlighted in Table 2. For the texture data, we show the results of the 10 combined SMO classifiers and the 10 combined k-NN classifiers

Table 4. Results of four CPs on the texture data. For each parameter we show the accuracy, and the certainty and error rates for three levels of confidence (95%, 85%, and 75%). We highlight the best results which are given by the average percentage of the accuracy and the certainty rates.

		Certainty			**Error**		
CP	**Acc.**	**95%**	**85%**	**75%**	**95%**	**85%**	**75%**
ANN neurons							
0	70.80%	34.67%	67.15%	88.69%	4.38%	12.77%	22.99%
1	69.34%	34.67%	67.15%	87.59%	4.74%	14.96%	24.09%
2	71.17%	32.12%	66.42%	86.50%	4.01%	14.23%	22.99%
3	70.07%	34.31%	66.79%	89.78%	4.38%	14.23%	24.82%
4	71.17%	33.21%	67.15%	90.15%	4.38%	13.50%	24.45%
5	70.07%	34.31%	66.42%	89.42%	4.74%	13.87%	24.45%
6	70.80%	32.85%	66.06%	89.05%	4.74%	13.50%	23.72%
7	71.17%	31.02%	67.15%	88.69%	4.01%	13.87%	22.99%
8	71.17%	33.94%	66.79%	89.78%	5.11%	13.50%	24.45%
9	71.53%	32.85%	67.52%	89.78%	4.74%	13.14%	24.09%
10	**71.53%**	**34.31%**	**67.15%**	**90.15%**	**4.74%**	**13.50%**	**24.09%**
SVM spread							
1	64.96%	17.88%	53.65%	77.74%	4.74%	14.96%	24.45%
2	68.25%	18.25%	55.84%	82.12%	4.74%	14.96%	24.45%
3	69.71%	25.55%	57.30%	81.02%	4.74%	14.96%	24.82%
4	69.71%	28.47%	55.47%	84.67%	4.74%	14.96%	24.82%
5	69.34%	28.83%	57.30%	84.67%	4.74%	14.96%	24.82%
6	69.71%	30.29%	59.85%	86.50%	4.74%	14.60%	24.82%
7	69.34%	31.39%	61.31%	86.86%	4.74%	15.33%	24.82%
8	69.34%	31.75%	61.68%	87.59%	4.74%	14.96%	24.82%
9	70.07%	31.75%	62.77%	87.96%	4.74%	14.96%	24.82%
10	**69.34%**	**32.12%**	**63.87%**	**88.32%**	**4.74%**	**14.96%**	**24.82%**
k-NN k							
20	70.07%	32.85%	68.98%	89.78%	4.74%	14.96%	24.82%
21	70.44%	33.21%	69.34%	89.05%	4.74%	14.96%	24.82%
22	70.07%	33.94%	69.34%	89.42%	4.74%	14.96%	24.82%
23	70.07%	33.94%	69.71%	89.42%	4.74%	14.96%	24.82%
24	70.80%	33.94%	69.71%	90.15%	4.74%	14.96%	24.82%
25	70.80%	33.94%	70.80%	90.15%	4.74%	14.96%	24.82%
26	**70.80%**	**34.31%**	**70.44%**	**90.15%**	**4.74%**	**14.96%**	**24.82%**
27	71.17%	33.94%	68.61%	90.15%	4.74%	14.96%	24.82%
28	71.53%	33.94%	68.61%	90.15%	4.74%	14.96%	24.82%
29	71.17%	33.58%	68.61%	90.15%	4.74%	14.96%	24.82%
30	71.53%	33.94%	68.61%	90.15%	4.74%	14.96%	24.82%
NBC							
—	69.34%	27.01%	57.66%	83.94%	4.74%	14.96%	24.82%

Table 5. Comparing Accuracy, True Negative Rate (TNR), and True Positive Rate (TPR) of four classifier algorithms with the corresponding CPs, on the texture data.

Method	Classifier			CP		
	Accuracy	**TNR**	**TPR**	**Accuracy**	**TNR**	**TPR**
ANN	68.97%	66.40%	71.50%	71.53%	66.12%	82.42%
SVM	69.70%	64.23%	75.18%	69.34%	63.50%	76.64%
NBC	70.07%	80.30%	59.90%	69.34%	74.77%	65.87%
***k*-NN**	70.43%	70.10%	70.80%	70.80%	65.69%	75.91%

Table 6. Comparing accuracy of the classifiers in Refs. 14 and 5 with the accuracy of our selected CPs on the morphological and texture data.

Method	Accuracy on Morphological Data	Method	Accuracy on Texture Data
SVM[14]	73.72%	**Comb. k-NN**[5]	68.8%
PNN[14]	70.44%	**Comb. SMO**[5]	73.1%
SVM-CP	73.72%	**k-NN-CP**	70.80%
ANN-CP	72.26%	**ANN-CP**	71.53%

used in Ref. 5. We compare these with our results of the k-NN-CP and ANN-CP as highlighted in Table 4. From the comparison, we are able to see that the accuracies on the morphological data and the texture data remain at about the same level with the accuracies of the two previous studies. Thus, we show that our CPs preserve accuracy while they provide important extra information (the confidence measures) for the expert physicians.

4.2.1. *Output for selected images*

One of the problems with current methods is the low percentage of correct classification results (around 70-75%). This is because of the nature of the problem. We are working on base line images, events recorded are for a period of eight years after images were captured. Thus, even though some of the plaques can be characterized by the experts as dangerous, we may have events that did not occur during the monitoring period. Instead, events may have occurred later or not at-all.

Figure 1 shows four plaques that were used in our experiments. Figure 1(a) shows a plaque that was classified as symptomatic by the ANN-CP, but with low confidence (70.80%). In this example, if we raise the required classification confidence above 70.80%, then the plaque classification changes to uncertain. The expert physician assessed this plaque as average risk. Thus, the CP classification, although wrong, shows low confidence in the prediction. A more accurate prediction is given in Figure 1(b). In this case, the plaque was classified as asymptomatic with very high

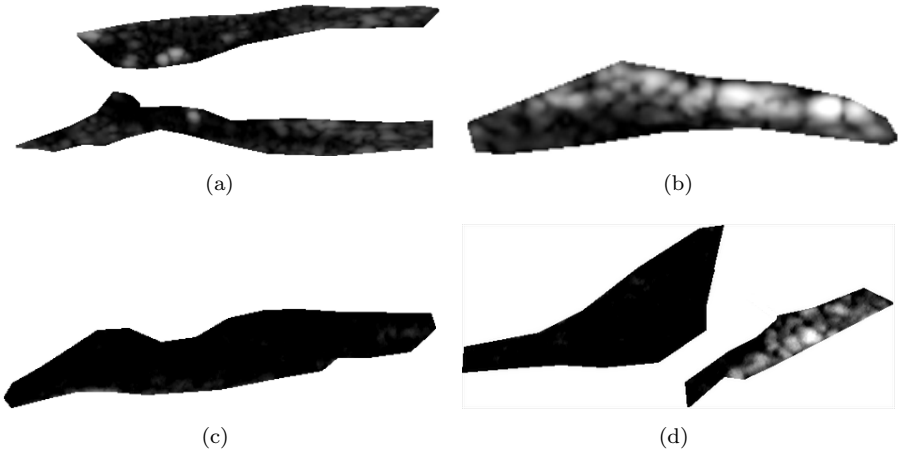

(a) (b)

(c) (d)

Fig. 1. (a) Plaque that was classified as low confidence (70.8%) symptomatic. The subject was asymptomatic but was classified as an average risk image by the expert physician. (b) Plaque that was classified as high confidence (99.64%) asymptomatic. This subject was asymptomatic and classified as low risk for symptoms by the expert physician. (c) Plaque that was classified as low confidence (69.34%) symptomatic. This subject had an AF event and was classified as low risk for stroke but high risk for AF by the expert physician. (d) Plaque that was classified as high confidence (99.64%) symptomatic. This subject had a stroke event and was classified as high risk for symptoms by the expert physician.

confidence (99.64%), in agreement with the expert physician. A symptomatic example is given in Figure 1(c). In this example, the plaque was classified as symptomatic but with low confidence (69.34%). If we raise the confidence requirement to above 69.34%, then the plaque classification changes to uncertain. However, this is one of the plaques that resulted in AF and was classified as low risk for stroke but high risk for AF by the expert physician. A more accurate symptomatic classification is given in Figure 1(d). In this example, the plaque was classified as symptomatic with high confidence (99.64%). Furthermore, this is a plaque associated with a stroke event and was identified as a dangerous plaque by the expert physician.

5. Conclusion

The classification of symptomatic and asymptomatic atherosclerotic plaques is a crucial task as it can be used to predict the risk of stroke. In this work, we have applied the Conformal Prediction framework on four machine learning algorithms in order to assign reliable confidence measures to the recognition of symptomatic or asymptomatic plaques; thus assess the risk of stroke. Our results demonstrate the validity of the produced confidence measures and their importance in the application of stroke prediction.

Critics point out that expert physicians are not familiar with the complex machine learning methods and tend to avoid using such methods widely. Therefore, a new step has to be made in order to allow for the expert physician to ignore

the underlying complex methodology and be able to trust the predictions of the machine. Our contribution in this work is exactly towards this aim. The proposed methods provide the expert physician with a reliable confidence measure for each prediction, which can be trusted based only on the i.i.d. assumption. As the confidence measures that we provide are valid (in the sense that they are proven to be correct), the expert physician needs to have no further knowledge about the methods in order to be able to trust the confidence measure in each prediction. In the future, we aim to improve the quality of our confidence measures by investigating other methods, while preserving the validity and the accuracy of the predictors.

References

1. Gianni Belcaro, Andrew N. Nicolaides, Giuseppe Laurora, Maria Rosaria Cesarone, Mariateresa De Sanctis, Lucrezia Incandela, and Antonio Barsotti. Ultrasound morphology classification of the arterial wall and cardiovascular events in a 6-year follow-up study. *Arterioscler Thromb Vasc Biol*, 16(7):851–856, 1996.
2. Tony Bellotti, Zhiyuan Luo, and Alexander Gammerman. Reliable classification of childhood acute leukaemia from gene expression data using confidence machines. In *Proceedings of IEEE International Conference on Granular Computing* (*GRC '06*), pages 148–153, 2006.
3. Tony Bellotti, Zhiyuan Luo, Alexander Gammerman, Frederick W. Van Delft, and Vaskar Saha. Qualified predictions for microarray and proteomics pattern diagnostics with confidence machines. *International Journal of Neural Systems*, 15(4):247–258, 2005.
4. Christodoulos I. Christodoulou, Efthyvoulos Kyriacou, Costantinos S. Pattichis, and Andrew Nicolaides. Multiple feature extraction for content-based image retrieval of carotid plaque ultrasound images. In *Proceedings of the 5th International IEEE Special Topic Conference on Information Technology Applications in Biomedicine*, pages 26–28, 2006.
5. C.I. Christodoulou, C.S. Pattichis, M. Pantziaris, and A. Nicolaides. Texture-based classification of atherosclerotic carotid plaques. *IEEE Transactions on Medical Imaging*, 22(7):902–912, 2003.
6. Devetyarov Dmitry and Nouretdinov Ilia. Prediction with confidence based on a random forest classifier. In *Artificial Intelligence Applications and Innovations – 6th IFIP WG 12.5 International Conference* (*AIAI 2010*), volume 339, pages 37–44. Springer Boston, 2010.
7. N. El-Barghouty, G. Geroulakos, A. Nicolaides, A. Androulakis, and V. Bahal. Computer-assisted carotid plaque characterisation. *European Journal of Vascular and Endovascular Surgery*, 9(4):389–393, 1995.
8. A. Gammerman, V. Vovk, and V. Vapnik. Learning by transduction. In *Uncertainty in Artificial Intelligence*, pages 148–155. Morgan Kaufmann, 1998.
9. Alexander Gammerman, Ilia Nouretdinov, Brian Burford, Alexey Chervonenkis, Volodya Vovk, and Zhiyuan Luo. Clinical mass spectrometry proteomic diagnosis by conformal predictors. *Statistical Applications in Genetics and Molecular Biology*, 7(2), 2008.
10. G. Geroulakos, A. Domjan, A. Nicolaides, J. Stevens, N. Labropoulos, G. Ramaswami, and G. Belcaro. Ultrasonic carotid artery plaque structure and the risk of cerebral infraction on computer tomography. *Journal of Vascular Surgery*, 20(2):263–266, 1994.

11. Arcangelo Iannuzzi, Timothy Wilcosky, Michele Mercuri, Paolo Rubba, Fred A. Bryan, and M. Gene Bond. Ultrasonographic correlates of carotid atherosclerosis in transient ischemic attack and stroke. *Stroke*, 26(4):614–619, 1995.
12. E.C. Kyriacou, C. Pattichis, M. Pattichis, C. Loizou, C. Christodoulou, S.K. Kakkos, and A. Nicolaides. A review of noninvasive ultrasound image processing methods in the analysis of carotid plaque morphology for the assessment of stroke risk. *Information Technology in Biomedicine, IEEE Transactions on*, 14(4):1027 –1038, 2010.
13. E.C. Kyriacou, C.S. Pattichis, M.A. Karaolis, C.P. Loizou, C.I. Christodoulou, M.S. Pattichis, S. Kakkos, and A. Nicolaides. An integrated system for assessing stroke risk. *Engineering in Medicine and Biology Magazine, IEEE*, 26(5):43–50, 2007.
14. Efthyvoulos Kyriacou, Marios S. Pattichis, Constantinos S. Pattichis, A. Mavrommatis, C. I. Christodoulou, S. Kakkos, and A. Nicolaides. Classification of atherosclerotic carotid plaques using morphological analysis on ultrasound images. *Applied Intelligence*, 30(1):3–23, 2009.
15. Antonis Lambrou, Harris Papadopoulos, and Alexander Gammerman. Reliable confidence measures for medical diagnosis with evolutionary algorithms. *IEEE Transactions on Information Technology in Biomedicine*, 15(1):93 –99, 2011.
16. Antonis Lambrou, Harris Papadopoulos, Efthyvoulos C. Kyriacou, Constantinos S. Pattichis, Marios S. Pattichis, Alexander Gammerman, and Andrew Nicolaides. Assessment of stroke risk based on morphological ultrasound image analysis with conformal prediction. In *Artificial Intelligence Applications and Innovations – 6th IFIP WG 12.5 International Conference* (*AIAI 2010*), pages 146–153, 2010.
17. M. Langsfeld, A.C. Gray-Weale, and R.J. Lusby. The role of plaque morphology and diameter reduction in the development of new symptoms in asymptomatic carotid arteries. *Journal of Vascular Surgery*, 9(4):548–557, 1989.
18. Thomas Melluish, Craig Saunders, Ilia Nouretdinov, and Volodya Vovk. Comparing the Bayes and Typicalness frameworks. In *Proceedings of the 12th European Conference on Machine Learning* (*ECML'01*), volume 2167 of *Lecture Notes in Computer Science*, pages 360–371. Springer, 2001.
19. Stavroula Gr. Mougiakakou, Spyretta Golemati, Ioannis Gousias, Andrew N. Nicolaides, and Konstantina S. Nikita. Computer-aided diagnosis of carotid atherosclerosis based on ultrasound image statistics, laws' texture and neural networks. *Ultrasound in Medicine & Biology*, 33(1):26 – 36, 2007.
20. Andrew N. Nicolaides, Edward G. Shifrin, Andrew Bradbury, Surinder Dhanjil, Maura Griffin, Gianni Belcaro, and Michael Williams. Angiographic and duplex grading of internal carotid stenosis: Can we overcome the confusion? *Journal of Endovascular Surgery*, 3(2):158–165, 1996.
21. Ilia Nouretdinov, Volodya Vovk, Michael Vyugin, and Alex Gammerman. Pattern recognition and density estimation under the general i.i.d. assumption. In David Helmbold and Bob Williamson, editors, *Computational Learning Theory*, volume 2111 of *Lecture Notes in Computer Science*, pages 337–353. Springer Berlin/Heidelberg, 2001.
22. Harris Papadopoulos. Inductive conformal prediction: Theory and application to neural networks. In Paula Fritzsche, editor, *Tools in Artificial Intelligence*, chapter 18, pages 315–330. I-Tech, Vienna, Austria, 2008. URL http://www.intechopen.com/download/pdf/pdfs_id/5294.
23. Harris Papadopoulos, Alex Gammerman, and Volodya Vovk. Reliable diagnosis of acute abdominal pain with conformal prediction. *Engineering Intelligent Systems*, 17(2-3):115–126, 2009.
24. Harris Papadopoulos and Haris Haralambous. Reliable prediction intervals with regression neural networks. *Neural Networks*, 24(8):842–851, 2011.

25. Harris Papadopoulos, Kostas Proedrou, Volodya Vovk, and Alex Gammerman. Inductive confidence machines for regression. In *Proceedings of the 13th European Conference on Machine Learning* (*ECML'02*), volume 2430 of *Lecture Notes in Computer Science*, pages 345–356. Springer, 2002.
26. Harris Papadopoulos, Vladimir Vovk, and Alex Gammerman. Regression conformal prediction with nearest neighbours. *Journal of Artificial Intelligence Research*, 40:815–840, 2011. URL http://dx.doi.org/10.1613/jair.3198.
27. Harris Papadopoulos, Volodya Vovk, and Alex Gammerman. Qualified predictions for large data sets in the case of pattern recognition. In *Proceedings of the 2002 International Conference on Machine Learning and Applications*, pages 159–163, 2002.
28. Harris Papadopoulos, Volodya Vovk, and Alex Gammerman. Conformal prediction with neural networks. In *Proceedings of the 19th IEEE International Conference on Tools with Artificial Intelligence* (*ICTAI'07*), volume 2, pages 388–395. IEEE Computer Society, 2007.
29. Kostas Proedrou, Ilia Nouretdinov, Volodya Vovk, and Alex Gammerman. Transductive confidence machines for pattern recognition. In *Proceedings of the 13th European Conference on Machine Learning (ECML'02)*, volume 2430 of *Lecture Notes in Computer Science*, pages 381–390. Springer, 2002.
30. Craig Saunders, Alex Gammerman, and Volodya Vovk. Transduction with confidence and credibility. In *Proceedings of the 16th International Joint Conference on Artificial Intelligence*, volume 2, pages 722–726, Los Altos, CA, 1999. Morgan Kaufmann.
31. Volodya Vovk, Alex Gammerman, and Craig Saunders. Machine-learning applications of algorithmic randomness. In *Proceedings of the Sixteenth International Conference on Machine Learning*, pages 444–453. Morgan Kaufmann, 1999.
32. Volodya Vovk, Alexander Gammerman, and G. Shafer. *Algorithmic Learning in a Random World*. New York, Springer, 2005.
33. J.E. Wilhjelm, M.-L.M. Gronholdt, B. Wiebe, S.K. Jespersen, L.K. Hansen, and H. Sillesen. Quantitative analysis of ultrasound b-mode images of carotid atherosclerotic plaque: correlation with visual classification and histological examination. *IEEE Transactions on Medical Imaging*, 17(6):910–922, 1998.